Urea-assisted morphological engineering of MFI nanosheets with tunable bthickness

Qiudi Yue, Chaowei Liu, Hongjuan Zhao, Honghai Liu, Pierre Ruterana, Jiaqi Zhao, Zhengxing Qin, Svetlana Mintova

Urea-assisted morphological engineering of MFI nanosheets with tunable b-thickness

Qiudi Yue[1], Chaowei Liu[2], Pierre Ruterana[3], Hongjuan Zhao[2], Honghai Liu[2], Jiaqi Zhao[4], Zhengxing Qin*[4], Svetlana Mintova[1,4]*

1. Laboratoire Catalyse et Spectrochimie, ENSICAEN, UNICAEN, CNRS, 14050 Caen, France
2. Petrochemical Research Institute, Petrochina Company Limited, 100195 Beijing, China
3. Centre de Recherche sur les Ions, les Matériaux et la Photonique, CIMAP-ENSICAEN, CNRS UMR 6252, 6 14050 Caen, France
4. State Key Laboratory of Heavy Oil Processing, College of Chemical Engineering, China University of Petroleum (East China), Qingdao, China

Correspondence: svetlana.mintova@ensicaen.fr; zhengxing.qin@upc.edu.cn

Abstract

Engineering of crystal morphology affects the catalytic and adsorption properties of zeolitic materials. Considering the anisotropic diffusion of molecules derived from its topological features, MFI nanosheets with short b-axis thickness are highly desired materials to reduce diffusion resistance. However, the design and development of eco-friendly synthesis protocols with reasonable cost and high efficiency remain elusive. Herein, we reported a systematic study on the synthesis of MFI nanosheets using urea as an additive. Both silicalite-1 and ZSM-5 zeolites (MFI type framework structure) with controllable b-thicknesses ranging from 50-100 nm were achieved by optimizing the synthetic parameters including water content, urea, and SDA concentration. The concentration of hydroxide anions was found to dominate the crystallization kinetics compared with the counterpart tetrapropylammonium cations (TPA^+). To facilitate the crystal growth of MFI zeolites in the presence of urea, the ratio OH^{-1}/SiO_2 has to be higher than 0.2, independent of the TPA^+ concentration. The role of urea in the assistance of plate-like crystal formation through the inhibition of (010) facet growth was revealed by electron microscopy and IR spectroscopy analyses. The developed strategy for morphological engineering is not limited to the MFI-type zeolite and can be applied to other frameworks depending on the intrinsic properties of additive molecules and the interactions between them.

Keywords: MFI zeolite, synthesis, nanosheets, additives, crystal morphology

Introduction

Zeolites are a family of crystalline microporous materials. The multiscale (*i.e.* from macro- to atomic-level) understanding of the zeolite chemistry including the morphology, framework topology, acidity, porosity, and chemical composition enhances its application in catalysis, adsorption, carbon capture, etc. [1]. For a given structure, any molecules whose dimensions are less than their sizes can have access to or leave their micropores. Nevertheless, mass transport is limited by slow molecule diffusion, which greatly affects reaction rates and reduces the useful fraction of the crystals [2]. As a result, the crystal morphology of zeolites significantly influences the end-use efficacy [3, 4]. Morphology engineering of zeolites resulting in hollow crystals [5], 2D zeolites [6], hierarchical zeolites [7], and nanosized zeolites [8], improves the diffusion-dependent catalytic properties of materials. Besides, zeolites with anisotropic channel systems also offer the manipulation of crystal morphology based on the characteristic feature of zeolite topology [9]. In other words, a small crystal size in that direction along which fast mass transfer occurs in channels is favored.

The MFI-type zeolites including pure siliceous Silicalite-1 and aluminum-containing ZSM-5 zeolite possess anisotropic channels, i.e., two types of 10-ring intersecting straight channels running in the *b*-axis and sinusoidal channels along the crystallographic *a* and *c* directions. ZSM-5 zeolite is the core catalyst in many important industrial processes owing to its unique shape selectivity, such as fluid catalytic cracking (FCC) [10], isomerization and disproportionation [11, 12], etc. However, a significant drawback is its catalyst deactivation caused by coke and pore blocking, which requires frequent regeneration of catalysts by calcination. Many advanced characterization techniques combined with theory discovered the anisotropic diffusion of molecules in the two kinds of channels of MFI zeolite, where diffusion in the sinusoidal channels is much slower than in the straight ones [13, 14]. Therefore, the diffusion limitation can be alleviated by reducing the mass transport distance along the *b*-axis. In other words, the MFI nanosheets with short b-thickness are particularly desirable.

The final crystal morphology is governed by both the intrinsic nature of the zeolite topology and many synthetic parameters, such as chemical composition, solvent, additives, crystallization temperature, etc. To restrict the growth rate along the *b*-axis of MFI zeolite, many strategies, as illustrated in Scheme 1, have been developed including 1) the design of novel organic structure-directing agents (OSDA) to prevent the stacking of extra pentasil layers, as a result, 1-2 pentasil-layered MFI zeolite is synthesized [15, 16]; 2) the use of fluoride anion promoting the plate-like crystal formation [17, 18], and the b-thickness of MFI crystals reaches down to around 10 nm [19, 20]; 3) the introduction of additive molecules to inhibit the growth along *b*-axis or promote the growth in other directions [21, 22]; and 4) the variation of the synthetic conditions, for

instance, gel composition, seeds, pH, and recrystallization, can also produce MFI crystal with short b-thickness [23-25]. A summary of developed methods regarding safety, cost, availability, and efficiency issues is presented. For instance, the safety, cost, and availability of the fluoride medium approach and complicated OSDA templates seem not compelling for industrial application, although they demonstrated to be highly efficient. Besides, controlling the synthetic conditions in either top-down or bottom-up approaches often requires multistep combinations of treatments and showed relatively low efficiency [26, 27].

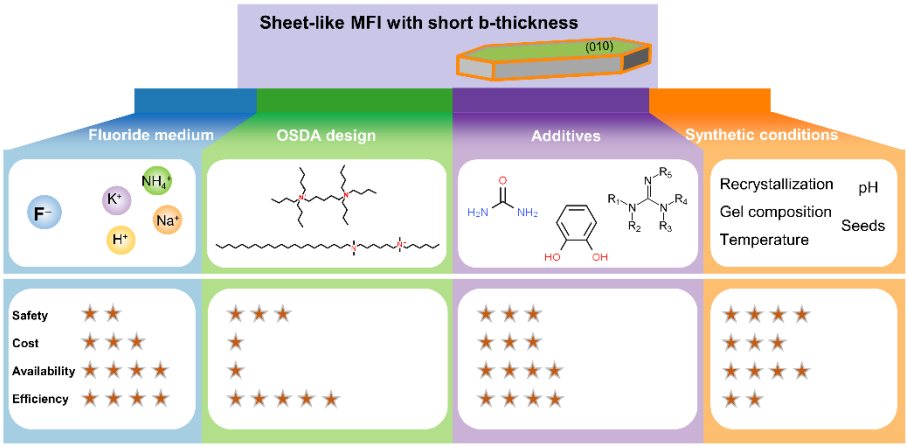

Scheme 1. Schematic presentation of the strategies available for the synthesis of MFI zeolite with short b-thickness; the number of stars shows an estimation of the safety, cost, availability, and efficiency of the methods. The more stars, the better.

The introduction of additive molecules into the synthesis gel is a promising approach to tailor the anisotropic growth rate of zeolites. These molecules interact either with a specific facet of zeolite crystals or with amorphous precursors regulating the kinetics of nucleation and growth, thus controlling the final crystal morphology [28]. Many additives varying from low-polarity hydrocarbons (*e.g.*, ketones) to high-polarity molecules (*e. g.*, acids, and amine compounds) have been used for the preparation of sheet-like MFI crystals [22, 29]. Generally, the molecules containing amine, hydroxide, and carbonyl groups are much more active than other hydrocarbons in regulating crystal morphology. Among them, urea is most considered owing to its relatively high efficiency and low cost [30-35]. It is suggested that urea molecules preferentially bind to (010) facet of MFI crystals to suppress its growth, resulting in a decreased b-thickness [30]. Recently, selective enrichment of urea molecules on the (010) facet of pre-formed MFI crystals by an ex-situ mechanistic study was reported [36]. Such preferential adsorption of urea is expected to contribute to the anisotropic growth of MFI zeolite. However, under synthetic hydrothermal conditions, the intrinsic role of urea responsible for the anisotropic growth remains elusive. In addition, the tailored synthesis of MFI nanosheets with

tunable b-thickness using urea through the optimization of synthetic conditions has not been explored yet.

In this work, the utilization of the urea additive for the preparation of MFI nanosheets combined with fine control of the gel nature (silica and alumina sources and water, urea, and SDA concentrations) and synthetic conditions were systematically studied. The initial focus was on the synthesis of pure siliceous MFI-type zeolite nanosheets (Silicalite-1), then the optimized approach was extended for the preparation of ZSM-5 zeolite. Through the optimization of the synthetic conditions, MFI nanosheets with b-thickness of 50-100 nm were prepared, and the role of urea responsible for the anisotropic crystal growth was also revealed.

2. Results and discussion

Urea additive was used in the synthesis of both pure siliceous (Silicalite-1) and Al-containing (ZSM-5) zeolites. The synthetic conditions were systematically studied and optimized as described in the experimental section.

2.1 Silicalite-1 synthesis in the presence of urea: the impact of gel concentration

The impact of gel concentration, *i.e.*, the water content, on the MFI crystal morphology in the presence of urea was studied using the following gel composition: 1 SiO_2: 0.36 TPAOH: 0.8 Urea: x H_2O; the H_2O/SiO_2 ratio was varied between 8 and 30. The crystallization of zeolites was carried out at 170 °C for 12 h. Three samples obtained from the precursor gels with different amounts of water (x = 8, 15, and 30) were subjected to X-ray diffraction (XRD) characterization. All these samples contain highly crystalline MFI zeolites (Figure S1). However, the microscopic examination of the samples by scanning electron microscopy (SEM) revealed that the MFI crystals are surrounded by amorphous particles in the sample with x = 30 (Figure S2), while the other two samples with x = 8 and 15 contain well-crystalline particles (Figure 1a-b). A further extension of the crystallization time to 18 h for the sample with x = 30 leads to the disappearance of the attached amorphous particles and a full crystallization of the sample (Figure 1c). The Ar physisorption study revealed the development of microporosity thus confirming the high crystallinity of samples. All these samples possess a type I isotherm expected for pure microporous materials (Figure S3). The micropore volume and the specific surface area were estimated to be 0.157–0.159 $cm^3\ g^{-1}$ and 494–504 $m^2\ g^{-1}$, respectively. Another interesting observation is that well-defined plate-like crystals synthesized with urea are obtained, in contrast to the reference sample containing crystals with a hexagonal prism

morphology (*vide infra*, see Figure 2b in section 2.3). In general, the size of the crystals decreased with decreasing the amount of water (Figure 1h).

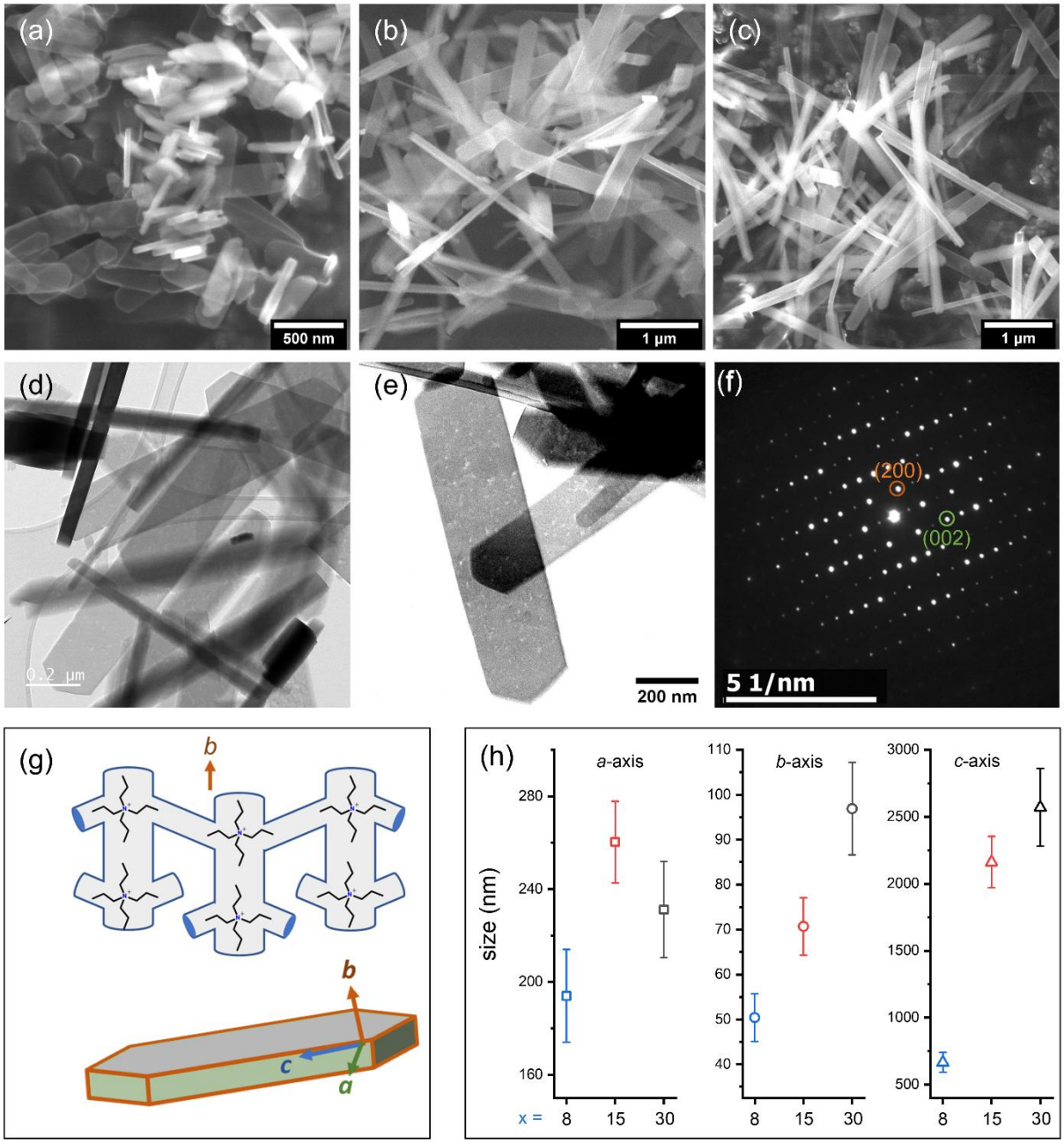

Figure 1. SEM images of silicalite-1 crystals synthesized from the precursor gel with a composition of 1 SiO_2/ 0.36 TPAOH/ 0.8 Urea/ x H_2O, where x = 8 (a), 15 (b), and 30 (c). The crystallization process of the samples with x = 15 and 8 was conducted at 170 °C for 12 h, while 18 h was used for the sample with x = 30. TEM images of the sample obtained with x = 8 in different magnifications (d-e), and the corresponding electron diffraction pattern from the "top" of nanosheets (f). Overview of the crystallographic orientation and channel system of MFI crystal (g). Statistical analyses of crystal sizes in the obtained samples synthesized from precursor gels with different water content (h).

The sample prepared with x = 8 was subjected to transmission electron microscopy (TEM) analysis to understand the crystal orientations. Well-defined plate-like crystals with a typical coffin-shaped morphology are shown in Figure 1d. The crystals have uniform sizes, and the thickness is about 50 nm. Interestingly, many mesopores homogeneously distributed can be observed in these crystals (Figure 1e), however, these pores were not detected by Ar physisorption analysis (Figure S3). This impales that the pores were likely generated by the electron beam during the TEM characterization. The selected area electron diffraction (SAED) pattern was taken perpendicular to the crystal sheet (Figure 1f), showing discrete spots indexed to the (200) and (002) planes of the MFI phase corresponding to the straight channels running along [010]. The coffin-shaped crystals with MFI-type framework structure possess a crystallographic *b*-axis with an exposed facet of [010] perpendicular to the crystal, while the crystallographic *a*- and *c*-axis run along the widened and elongated directions, respectively (Figure 1g). This observation is consistent with previous reports [9, 19, 37].

Statistical analyses of the lengths in three directions for the obtained crystals were performed using the SEM images, and the data are presented in Figure 1h. The b-thickness of MFI nanosheets decreases from 97 to 50 nm as the x decreases to 8. The L_c/L_b values decrease from 30.6 to 13.2 in response to the decrease of the H_2O/SiO_2 ratio, while L_c/L_a ratio rises from 8.3 to 11.1 before dropping to 3.4. With the exception of 2.4 for the sample with x = 15, the L_a/L_b aspect ratios are remarkably comparable (3.7-3.8). In summary, the alteration of gel concentration (water content) was found to mainly affect the relative growth rate along the *c*-axis, i.e. the more dilute gel the larger size of crystals was obtained. This observation can be explained by faster polymerization of D5R silicate anions into pentasil chains (longer *c*-length) due to the presence of D5R silicate anions favored at low pH [38, 39] and/or slow crystallization kinetics resulting in the formation of larger crystals in dilute gels [40].

2.2 Silicalite-1 synthesis in the presence of urea: the impact of urea concentration

The impact of urea concentration on the crystal morphology was investigated using the precursor gel with the following composition: 1 SiO_2: 0.36 TPAOH: y Urea: 8 H_2O, where y was varied in the range of 0–0.8. Independent of urea concentration, all the obtained materials show highly crystalline MFI zeolites, as indicated by the XRD patterns depicted in Figure 2a. On the other hand, the morphology of crystals is found to be dependent on the amount of urea used. In the reference sample without the addition of urea additive (y = 0), silicalite-1 crystals with a typical hexagonal prism morphology were produced (Figure 2b). When a small amount of urea (y= 0.1) was added, the crystals lost the regular prismatic features and turned into irregular ellipsoids (Figure 2c). When y was increased to 0.5, and further to 0.8, well-shaped

MFI nanosheets were obtained (Figures 1a and 2d). We also analyzed the crystal sizes of nanosheets collected from samples with y = 0.5 and 0.8 and it is found that the length in three directions is very similar (Figure S4). Therefore, although urea serves as a key modulator for MFI anisotropic growth, unlike the strong influence of water on the crystal aspect ratios, a further increase in the amount of urea (y > 0.5) does not change substantially the morphology of MFI crystals, similar to the fluoride anion used for the synthesis of plate-like MFI crystals [19].

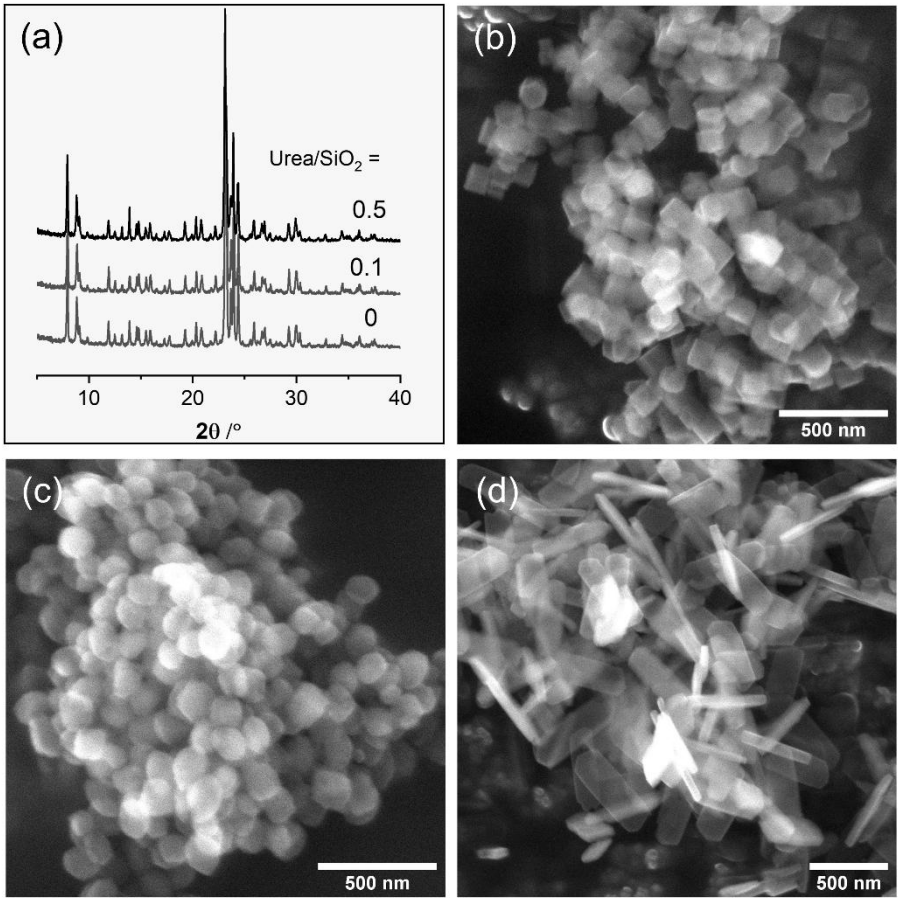

Figure 2. XRD patterns (a) and SEM images of silicalite-1 synthesized from the precursor gel with a composition of 1 SiO_2/ 0.36 TPAOH/ y Urea/ 8 H_2O at 170 °C for 12 h, with y = 0 (b), 0.1 (c), and 0.5 (d).

2.3 Silicalite-1 synthesis in the presence of urea: the impact of OSDA concentration

To study the effect of OSDA concentration on the crystal morphology in the presence of urea, the synthesis in a gel with a composition of 1 SiO_2: z TPAOH: 0.8 Urea: 8 H_2O, with z = 0.05–0.36 at 170 °C for 24 h was performed. As shown in Figure 3a, crystalline MFI zeolite can be obtained only with z = 0.36, while at lower TPA^+ concentrations (*i.e.*, $z \leq 0.2$) the products remain amorphous. The obtained materials after 24 h crystallization contain small particles corresponding to amorphous silica if $z \leq 0.2$, while the MFI nanosheets were obtained at z =

0.36 (Figure 3b-d), the crystallization time was even as short as 3 h (see section 2.2). These results indicate the crystallization kinetics shift when the urea is used, especially at low TPAOH concentrations.

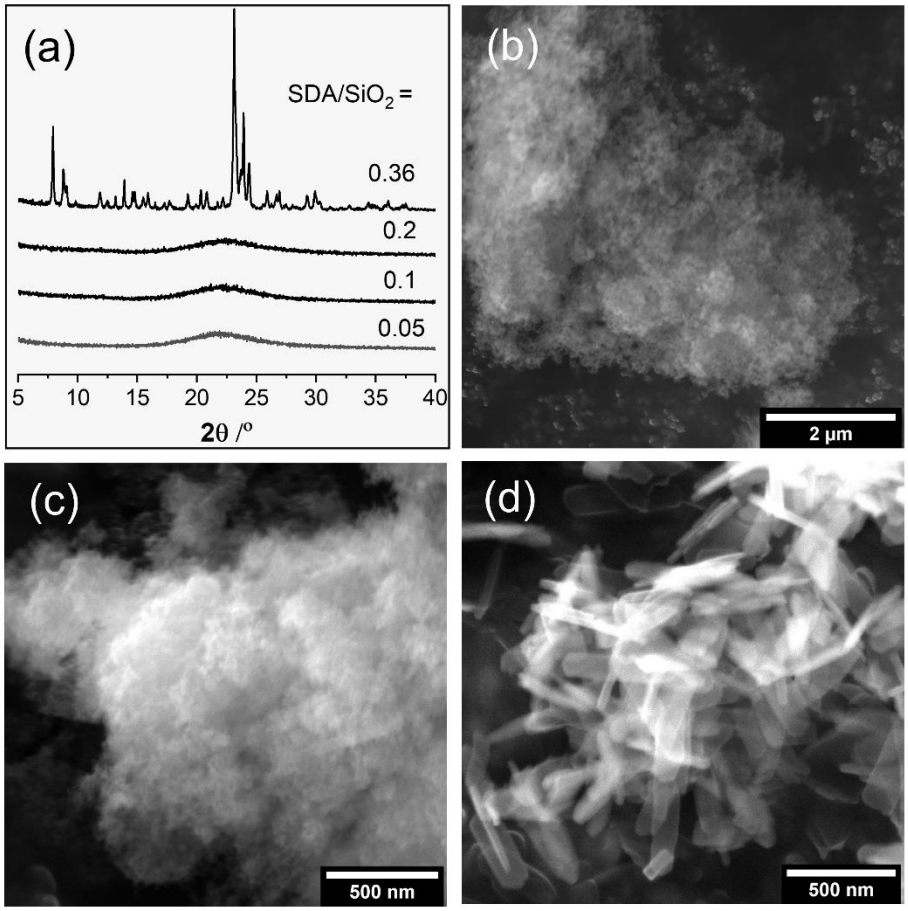

Figure 3. XRD patterns of samples obtained from the precursor gel with a composition of 1 SiO_2: z TPAOH: 0.8 Urea: 8 H_2O at 170 °C for 24 h with z = 0.05 – 0.36 (a). SEM images of selected examples with z = 0.05 (b), 0.2 (c), and 0.36 (d).

The increase of the TPAOH concentration in the precursor gel introduces two variables in the system, the TPA^+ and OH^-, and both can affect the zeolite crystallization. To find out the determinant factor that controls the zeolite formation either TPA^+ or OH^- in the presence of urea [41], part of the TPAOH was replaced by TPABr, while maintaining other synthesis parameters unchanged. A solid precursor before hydrothermal treatment was formed after TEOS hydrolysis when 0.16 equiv. TPAOH plus 0.2 equiv. TPABr was used, while a liquid gel was obtained when using TPAOH solely (Figure 4a). Different from the crystalline $product_{[TPAOH]}$, the $product_{[TPAOH+TPABr]}$ remains amorphous after 24 h crystallization at 170 °C (Figure 4b). The $product_{[TPAOH+TPABr]}$ is composed of small silica particles as shown in Figure 4c. Although several plate-like crystals can be found (crystallinity < 1%, Figure S5), however, further prolongation of

the crystallization time to 3 days did not generate fully crystalline materials (crystallinity < 50%, Figure S6) indicating slow crystallization kinetics.

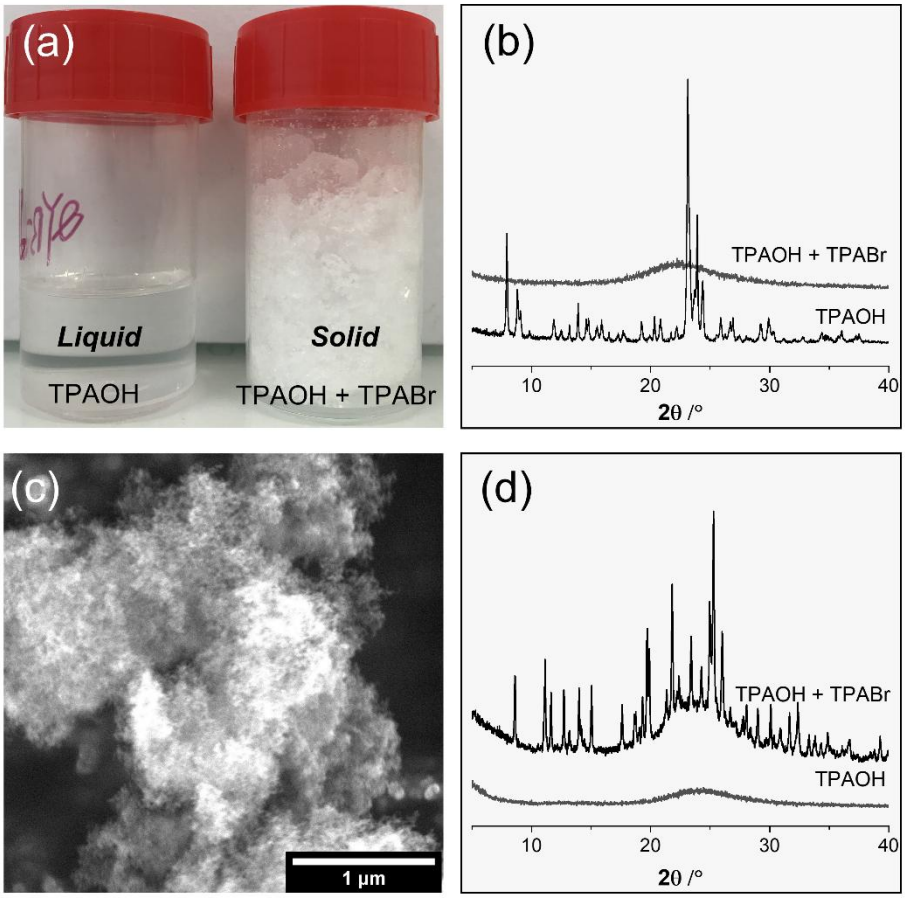

Figure 4. Photograph of the precursors before hydrothermal synthesis with gel compositions of 1 SiO_2: [(0.16 TPAOH+ 0.2 TPABr) or 0.36 TPAOH]: 0.8 Urea: 8 H_2O; a *solid* precursor formed when both 0.16 TPAOH and 0.2 TPABr were used and a *liquid* precursor formed when 0.36 TPAOH was used solely (a). XRD patterns of the samples obtained at 170 °C for 24 h from the *solid* and *liquid* precursors, respectively (b). SEM image of the sample obtained at 170 °C for 24 h from the *solid* precursor (c). XRD patterns of the *solid* and *liquid* freeze-dried precursors before hydrothermal synthesis (d).

It is well known that TPAOH is able to direct the formation of MFI zeolite even under extremely low concentrations (e.g. TPA^+/SiO_2 = 0.002; Ref. [32]). To understand the slow crystallization process of zeolites when urea is present at low concentrations of hydroxide anions, the synthesis precursors prior to the hydrothermal treatment were examined by XRD. Surprisingly, the liquid precursor (*i.e.*, z = 0.36 TPAOH) is amorphous while the solid precursor (z = 0.16 TPAOH + 0.2 TPABr) shows intense Bragg diffraction peaks (Figure 4d). Although the assignment of the crystalline phase is complicated [42], we can infer from the peak positions (mainly located at 10–30°) that it contains crystalline organic/inorganic silicate compounds. With high hydroxide anions concentration (OH^{-1}/SiO_2 > 0.2), the formed silicate compounds are highly

hydrated, mobile, and disordered. On the other hand, the precursor is solidified and immobile at low concentrations of hydroxide anions ($OH^{-1}/SiO_2 \leq 0.2$). The solid precursor with highly decreased silicate solubility polymerizes and leads to the formation of MFI zeolite crystals following the slow crystallization kinetics. To increase the silica mobility [43], fluoride anion was introduced into the precursor gel. As a result, crystalline MFI zeolite is formed in 6 h even at z = 0.1 (Figure S7).

2.4 Silicalite-1 synthesis in the presence of urea: the impact of crystallization time

The time required for complete crystallization of MFI-type crystals in the presence of urea additive was investigated using a precursor gel with a composition of 1 SiO_2: 0.36 TPAOH: 0.8 Urea: 8 H_2O; the hydrothermal synthesis was carried out at 170 °C for different times (0–280 min). Intermediate products were sampled at 70, 90, 125, 180, and 280 min of crystallization carried out in a static oven. Before any measurements (*e.g.* XRD, TEM, IR), the products were freeze-dried under a vacuum prior to purification (washing).

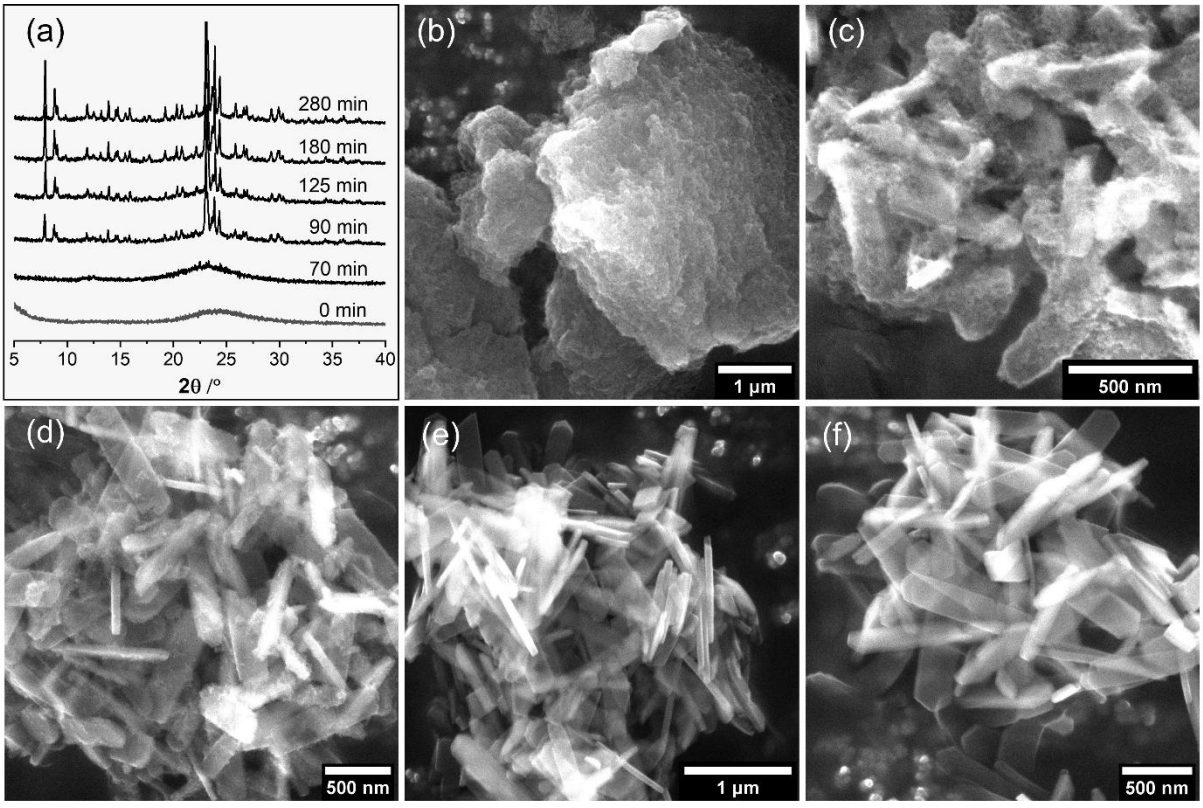

Figure 5. XRD patterns of products synthesized from the precursor gel with a composition of 1 SiO_2: 0.36 TPAOH: 0.8 Urea: 8 H_2O at 170 °C for 70–280 min (a). SEM images of the samples obtained after 70 (b), 90 (c), 125 (d), 180 (e), and 280 min (f) hydrothermal treatment.

The emergence of MFI diffraction peaks in the sample after 70 min induction period was confirmed by XRD, and the crystallization process was completed after 180 min (Figure 5a). In agreement with the improved crystallinity of the samples, only agglomerated small amorphous particles were observed after 70 min (Figure 5b). Noteworthily, after the induction period, the crystallization rate of the MFI zeolite was very fast as evident from the intensive Bragg peaks observed in the XRD pattern of the sample after 90 min. The incomplete plate-like crystals are obtained after 90 min accompanied by the presence of amorphous particles (Figure 5c). The nanosheet crystals grew by the consumption of the residual silica particles, and the fully crystalline sample was obtained after 180 min (Figure 5d-f). The yield of the crystalline product obtained after 3 h hydrothermal treatment was found to be nearly 100%. The high crystalline yield was also evidenced by the absence of amorphous particles on the smooth surface of the nanosheet crystals even without any purification (Figure 5e-f).

Both the XRD patterns (Figure 5a) and Ar physisorption isotherms (Figure S8) prove the high crystallinity of the sample after 180 min hydrothermal treatment. The micropore volume of the sample obtained in 3 h is 0.16 $cm^3\ g^{-1}$ which is comparable with the sample crystallized for 12 h (see Figure S3). No difference in the micropore volume for the samples obtained after 3 and 12 h was observed indicating that well-crystalline material can be synthesized even in 3 h. Besides the micropores of MFI crystals (0.55 nm), pores with a dimension of 0.9 nm were observed. Further prolongation of the crystallization process to 5-12 h did not lead to significant morphological changes in the crystals (Figure S8).

2.5 Synthesis of Silicalite-1 in the presence of Urea: mechanistic study

The crystallization process of MFI nanosheets in the presence of urea was also studied by FTIR spectroscopy in the ATR mode. Data were collected from as-synthesized samples prior to purification. The spectra in the range of 650–1800 cm^{-1} are shown in Figure 6. The assignment of the IR bands is difficult considering the presence of non-reacted silica, urea, TPA^+, H_2O, and decomposed components during the hydrothermal process. For example, the CH_2 bending and C-N stretching vibrations from both TPA^+ and urea can be found in this region [44-46]. Besides, the spectral range of 1600–1700 cm^{-1} contains the OH bending vibrational bands of adsorbed water [47, 48], the C=O stretching, and N-H deformation vibrational bands from urea and its decomposed products [46, 49, 50]. The contribution from the aforementioned components (urea, TPA^+, and non-reacted amorphous silica) was further confirmed by recording the spectra of samples after purification. No vibrational bands in the 1300–1700 cm^{-1} region for the washed samples were observed (Figure S9). In addition, bands assigned to the Si–O in-plane stretching vibrations of the silanol groups at around 970 cm^{-1} almost disappeared [51].

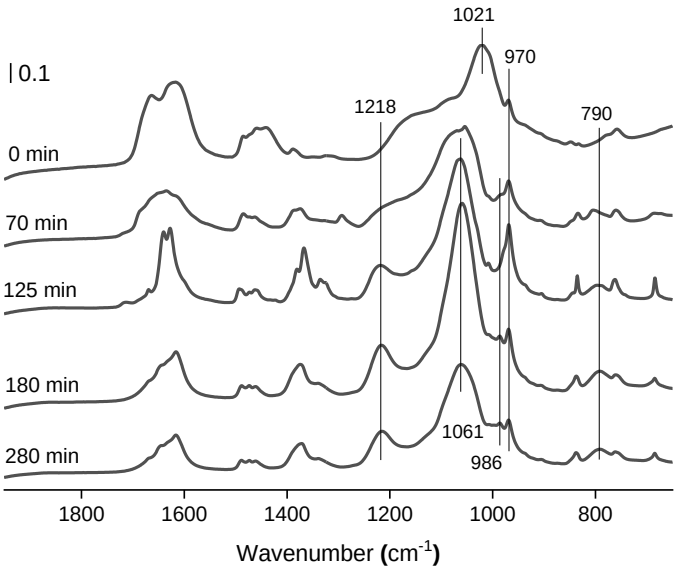

Figure 6. FTIR spectra of non-purified samples from the precursor gel with a composition of 1 SiO_2: 0.36 TPAOH: 0.8 Urea: 8 H_2O at 170 °C for 0–280 min; spectra recorded in the ATR mode.

The evolution of crystal formation was analyzed by following the change of Si–O vibrational bands as a function of the crystallization time [52]. The IR spectrum of the sample prior to hydrothermal treatment (0 min) contains no framework Si–O vibrational bands and only one strong band centred at 1021 cm^{-1} corresponding to amorphous silica is present [53]. Under hydrothermal treatment of the samples, the IR band centred at 1021 cm^{-1} shifts to higher wavenumbers. For the sample treated for 70 min, the vibrational Si–O–Si band is centred around 1060 cm^{-1} accompanied by the disappearance of the broad band at 1160 cm^{-1} [51, 53]. Therefore, although it is considered amorphous under X-ray inspection (Figure 5a), the material after crystallization for 70 min can be regarded as quasi-ordered material. The band at 1061 cm^{-1} corresponding to the asymmetric stretching vibration became sharper for the samples subjected to longer hydrothermal treatment indicating the formation of crystalline MFI zeolite [54]. Apart from the band at 1061 cm^{-1}, the appearance of another asymmetric stretching vibrational band at 1218 cm^{-1} and the symmetric stretching vibrational band at 790 cm^{-1} also confirmed the development of MFI structure [54, 55]. This behavior was also confirmed by FTIR study performed on purified zeolite samples (Figure S9).

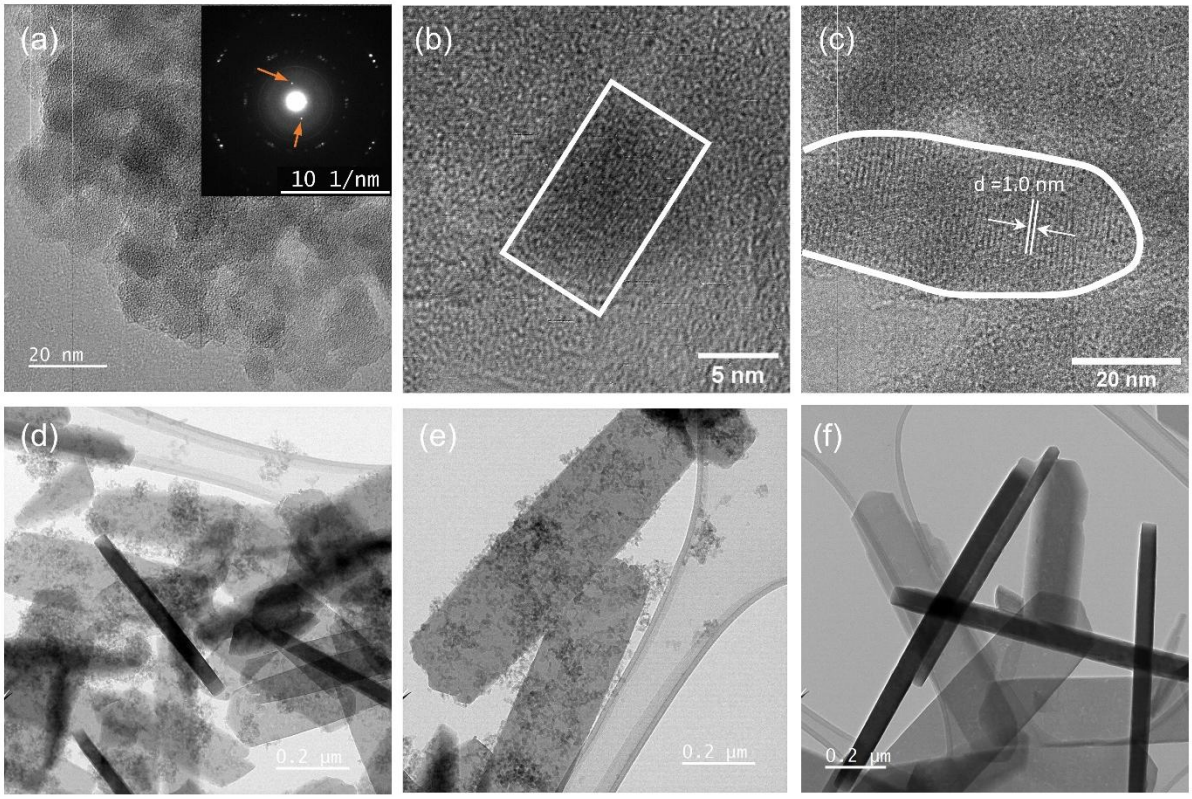

Figure 7. TEM images collected from the precursor gel with a composition of 1 SiO_2: 0.36 TPAOH: 0.8 Urea: 8 H_2O after crystallization at 170 °C for 70 min (a-c), 90 min (d), 125 min (e), and 180 min (f). The insert SAED pattern was recorded for the sample after 70 min crystallization.

The crystal growth process was further followed by transmission electron microscopy (TEM) analysis. Many crystallites were observed between these heavily agglomerated small particles after 70 min crystallization (Figure S10), although they amorphized fast under the electron beam. The SAED pattern confirms the presence of a crystalline phase together with the amorphous phase (Figure 7a), which is in line with the IR results. Noteworthily, instead of being round- or square-shaped, rectangle-shaped crystallites are present (Figure 7b-c and Figure S10). It is an important observation that urea plays the role of regulator of crystal orientation at the very early stage of crystal growth, different from the fluorine agent that affects the anisotropic growth on the surface of pre-formed MFI seeds [19, 20]. Promoted by the urea these crystallites continue to grow, and plate-like crystals are obtained after 90 min, surrounded by a large number of small particles (Figure 7d). In addition, the (101) facets in the two ends of the incomplete crystals have not appeared yet before reaching their maximum *c*-length in the discrete crystals (Figure 7d-e). This suggests the inhibition effect of urea that selectively adsorbed on the (010) facets of MFI to suppress its growth, being responsible for plate-like crystal formation, otherwise, the (101) facets are likely to be formed caused by the promotion effect [36]. This is different from the fluoride or H-amine-containing systems where the (101)

facet forms and is presented during the crystal growth [20, 36]. During the continuous crystallization, the well-shaped MFI nanosheets are formed and the small amorphous particles were fully consumed (Figure 7f).

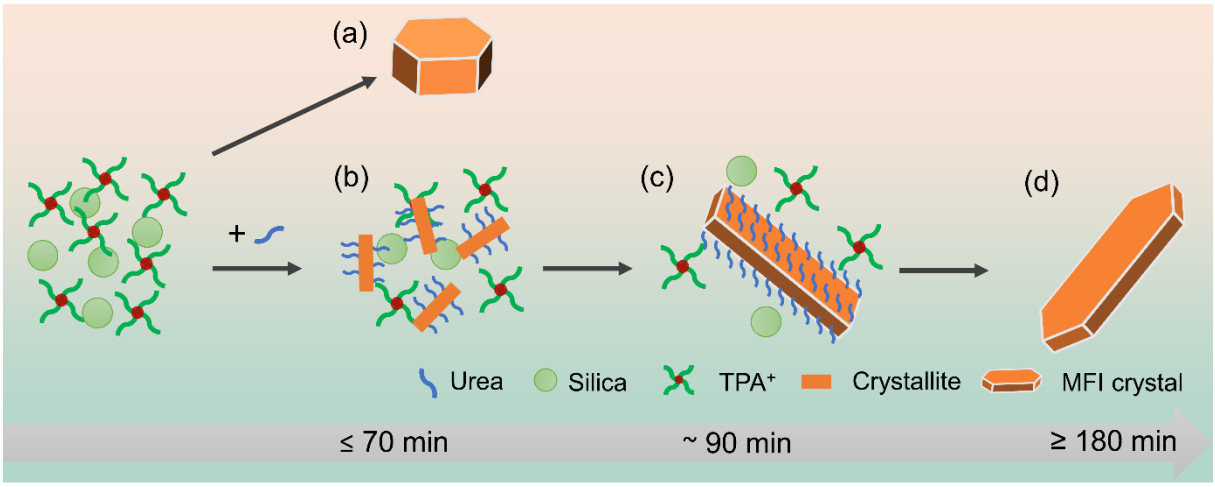

Scheme 2. Schematic presentation of the MFI crystallization in the absence or presence of urea as an additive. Hexagonal prism crystals were obtained in the absence of urea (a). When the urea additive was added, the crystallization process follows the formation of the rectangular crystallites after about 1 hour (b), then the growth of nanosheet crystals with unfinished two ends (c), and finally coffin-shaped MFI nanosheets were formed (d).

The crystallization pathway of silicalite-1 in the presence or absence of urea additive is illustrated in Scheme 2. The continuous growth of MFI-type zeolite under hydrothermal treatment relies on the condensation of silicate anions around the TPA^+ cations on the surface of the crystals. It was found that the interaction between the $[SiO_{4/2}F]^-$ unit and TPA^+, resulting in the alteration of TPA^+ orientation in the cavities, was responsible for nanosheet formation in the fluorine medium [20]. In our case, the adsorption of urea mainly on the (010) facet interferes with the TPA^+ ions resulting in slow deposition of silicate on the surface. This decreases the crystal growth rate of (010) facet, resulting in the formation of (010) oriented plate-like crystals. In addition, the interaction between the urea and TPA cations may influence the TPA orientation in the zeolite pores, thus is considered to be impactful on the pore-developing direction along *a*- and *b*-axes compared to the densely packed pentasil chain along the *c*-axis [56]. Therefore, a linear relationship of L_a/L_b is anticipated if the influence along both *a*- and *b*-axes are similar. In our case, we found that the L_a/L_b is 3-4, which is in good agreement with the previous report [56].

2.6 ZSM-5 synthesis in the presence of urea

The developed synthesis approach was extended to the preparation of ZSM-5 nanosheets. Considering that the ZSM-5 zeolites can be synthesized using a variety of Si and Al sources, the impact of Si and Al sources on the crystal morphology was also investigated. Specifically, the composition of the precursor gel was selected to be 1 SiO_2: 0.01 Al_2O_3: 0.36 TPAOH: 0.8 Urea: 8 H_2O for the preparation of ZSM-5 crystals using TEOS, colloidal silica, and fumed silica as Si sources, while $Al_2(SO_4)_3$, $Al(OH)_3$, and Al(O-i-Pr)$_3$ as Al sources; the crystallization was carried out at 170 °C for various times.

All samples contain highly crystalline MFI zeolites, as indicated by XRD patterns presented in Figure S11. Although the same synthesis recipe was applied, the crystal morphology and size of the products varied depending on the Si and Al sources used. The SEM images of the samples are shown in Figure 8. According to the morphological features, the samples can be classified into three groups: (i) plate-like single crystals (Figure 8a, b, c and e), (ii) 90°–twinned single crystals (Figure 8d, f and g), and (iii) 90°–twinned polycrystalline particles (Figure 8h and i). Products made from TEOS as Si source and independent of the Al source and colloidal silica with $Al(OH)_3$ exhibit plate-like single crystals, while products from other two colloidal silica, fumed silica with $Al_2(SO_4)_3$ belong to the category of 90°–twinned single crystals, the rest two samples prepared from fumed silica contain 90°–twinned polycrystalline crystals. The Si and Al sources determine the crystallization kinetics of the ZSM-5 formation. The crystallization rate is much faster when TEOS or colloidal silica was used in comparison to the fumed silica, however, there is one exception if $Al(OH)_3$ was utilized, which is probably caused by the low solubility of $Al(OH)_3$.

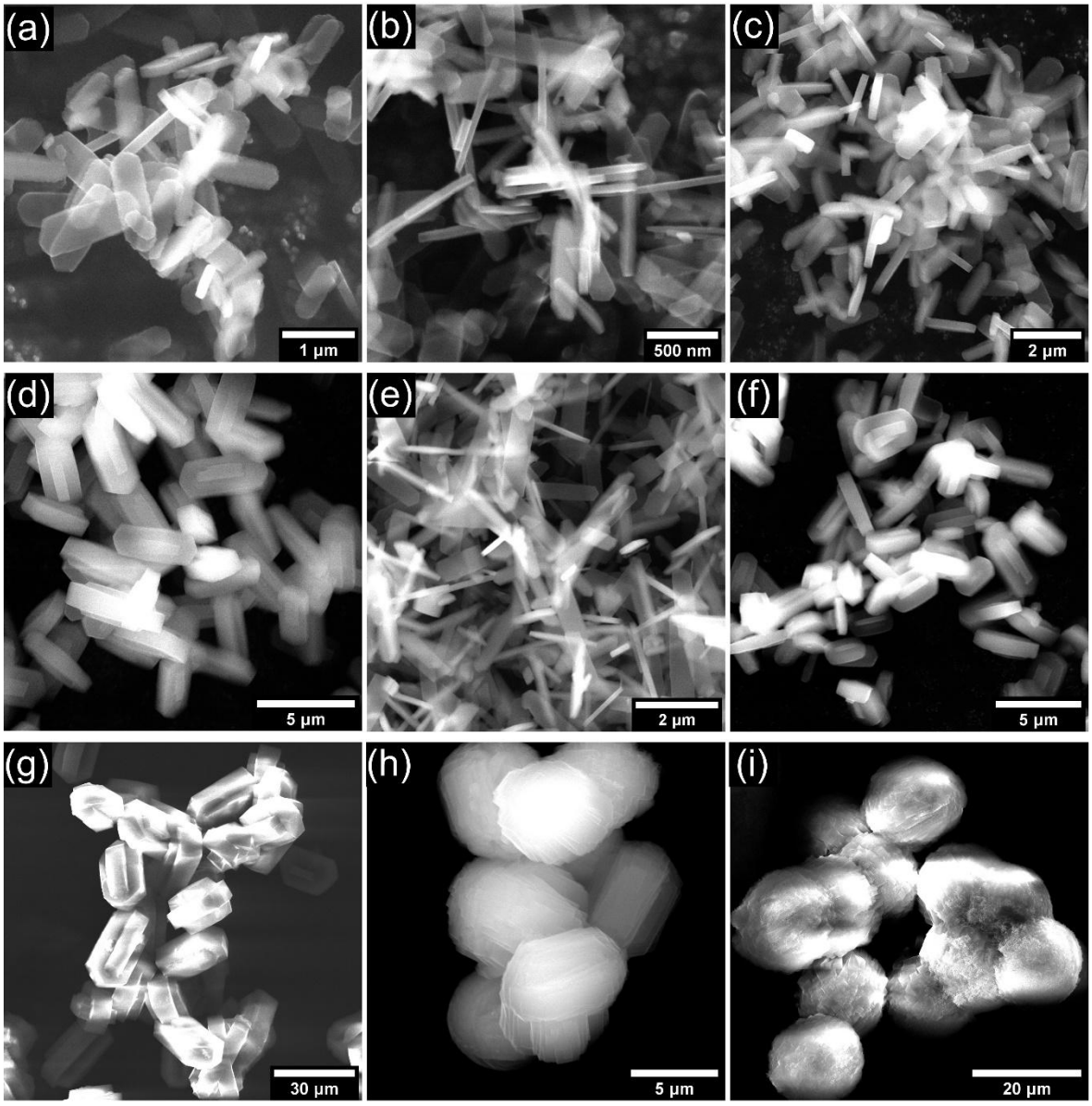

Figure 8. SEM images of ZSM-5 crystals synthesized from the precursor gel with a composition 1 SiO_2: 0.01 Al_2O_3: 0.36 TPAOH: 0.8 Urea: 8 H_2O at 170 °C using different Si and Al sources: TEOS + $Al_2(SO_4)_3$ (a), TEOS + $Al(OH)_3$ (b), TEOS + $Al(O\text{-}i\text{-}Pr)_3$ (c), colloidal silica + $Al_2(SO_4)_3$ (d), colloidal silica + $Al(OH)_3$ (e), colloidal silica + $Al(O\text{-}i\text{-}Pr)_3$ (f), fumed silica + $Al_2(SO_4)_3$ (g), fumed silica + $Al(OH)_3$ (h), fumed silica + $Al(O\text{-}i\text{-}Pr)_3$ (i). Crystallization time: a, 24 h; b, 270 h; c, 24 h; d, 24 h; e, 270 h; f, 24h; g, 173 h; h, 173 h; i, 270 h.

The statistical analysis of the sizes of plate-like ZSM-5 crystals is presented in Figure S12. As shown, the ZSM-5 zeolite crystals are larger than the silicalite-1 (Figure 1). The lengths in the *a*- and *c*-axis axes vary in the range of 200–640 nm and 900–2200 nm, respectively. The thicknesses of crystals along the *b*-axis are between 60 and 200 nm. The *b*-axis for ZSM-5 samples changed in the order b < a < e < c (samples labeled in Figure 8). The L_a/L_b ratio of the

samples is similar (3.2–4.0), in agreement with the above results, while the L_c/L_b ratio varies between 10 and 18 in the order e > b > a > c.

3. Conclusions

In this work, we demonstrate that adding urea to regulate crystal growth orientations is an efficient approach for the preparation of zeolite of particular plate-like morphology. The synthetic parameters, including the amount of water, urea, and SDA, with adjustment of the crystallization time, were systematically investigated and optimized towards the synthesis of MFI zeolites with tunable *b*-thickness. As a result, MFI nanosheets of typical coffin shape including silicalite-1 and ZSM-5 with controllable b-thickness in the range of 50-200 nm were synthesized.

The results show that urea starts to regulate the anisotropic growth at the early nucleation step, resulting in the formation of rectangular-shaped crystallites, and the following crystal growth rate was found to depend on the crystal facets. The growth along the *b*-axis can be significantly suppressed and the effect of the optimization of synthesis parameters (physical and chemical) on the (100) and (010) is synchronized. It is demonstrated that a large amount of hydroxide anions (OH^{-1}/SiO_2 = 0.36) is required to stimulate the zeolite crystallization when urea is participated in, otherwise, at $OH^{-1}/SiO_2 \leq 0.2$ the crystal growth rate is slow. Fast crystallization of silicalite-1 is observed in 3 h, at high hydroxide anions concentration.

In the synthesis of ZSM-5 zeolites with urea, the Al increases to some extent as well as the size of the crystals increased in comparison to the silicalite-1. In addition, the silica and aluminum sources were found to affect the final crystal morphology. The ZSM-5 samples prepared using TEOS as Si source independent of the Al source, and colloidal silica combined with $Al(OH)_3$ contain plate-like single crystals.

Methods

4.1 Materials

Urea, ≥99%, Sigma-Aldrich; Tetrapropylammonium hydroxide solution (1M), Alfa Aesar; Tetraethyl orthosilicate (TEOS), ≥99%, Sigma-Aldrich; Colloidal silica, HS-40, LUDOX; Fumed silica, AEROSIL®130 Evonik; Aluminum sulfate octadecahydrate ($Al_2(SO_4)_3 \cdot 18H_2O$), ≥97%, Sigma-Aldrich; Aluminum hydroxide ($Al(OH)_3$), extra pure, ACROS; Aluminium isopropoxide (Al(O-i-Pr)$_3$), ≥99%, Thermo Scientifc.

4.2 Synthesis of silicalite-1

To systematically study the role of the urea additive in the promotion of MFI nanosheet formation, substantial work has been executed to adjust the ratios between different reactants, crystallization temperature, and time. The precursor gel composition for the preparation of the siliceous MFI (silicalite-1) samples was 1 SiO_2: z TPAOH: y Urea: x H_2O, where x = 8–30, y = 0–0.8, z = 0.05–0.36; the crystallization was performed at 170 °C for 0–24 h. For a typical synthesis with x = 8, y = 0.8, and z = 0.36, 1.92 g urea was dissolved into 14.4 g 1M TPAOH solution, 8.33 g TEOS was added, and then hydrolyzed at room temperature overnight. After that, the temperature was increased to 45 °C to evaporate the ethanol and water (5.7 g) to reach the desired water content. When reaching the desired composition, the gel was transferred into a Teflon-lined autoclave and then put at 170 °C in a static oven. The products were purified with double distilled water using a high-speed centrifuge. Then the samples were dried at 60 °C in an oven overnight. The zeolite samples were calcined at 550 °C for 6 h prior to characterization.

4.3 Synthesis of ZSM-5

ZSM-5 samples were synthesized from the precursor gel with a composition of 1 SiO_2: 0.01 Al_2O_3: 0.36 TPAOH: 0.8 Urea: 8 H_2O. TEOS, colloidal silica, and fumed silica, and $Al_2(SO_4)_3$, $Al(OH)_3$, and $Al(O\text{-}i\text{-}Pr)_3$ were used as Si and Al sources, respectively. The procedures for preparation of the precursor gel, crystallization, and purification were the same as for silicalite-1 samples, except for the dissolution of Al sources before adding the urea into the TPAOH solution.

4.4 Characterization

Powder X-ray diffraction (PXRD) patterns were collected with a PANalytical X'Pert Pro diffractometer using Cu Kα1 radiation (λ = 1.5406 Å, 45 kV, 40 mA). Scanning electron microscopy (SEM) study was performed using a Tescan Mira I LMH under 30 kV. The analysis of zeolite crystal size was performed by measuring each sample along three axes with at least ten crystals with appropriate orientation. The N_2 adsorption/desorption isotherms were recorded at -196 °C on a Micromeritics 3Flex Surface Characterization unit. The samples were outgassed under vacuum at 450 °C for at least 8 h before measurement.

ATR-IR spectra were collected using a FTIR spectrometer (Nicolet iS50) equipped with a liquid nitrogen-cooled MCT detector coupled with a Specac Golden Gate ATR device that provides a diamond crystal (as an Internal Reflection Element (IRE)) with one reflection beam at 45°. The background was taken before the sample measurement (32 scans collected with a resolution of 4 cm^{-1}). Freeze-dried non-purified and purified zeolite samples were subjected to FTIR measurements.

Transmission electron microscopy (TEM) was carried out on F200 JEOL microscope equipped with a fast detection camera in order to minimize the effects of electron beam damage. The samples were prepared by dispersing zeolite powders on copper grids with holey graphenic carbon.

5. Acknowledgements

The authors acknowledge Luis J. Aguilera for the measurement of ATR-FTIR spectra, and Marie Lozier for Ar physisorption measurement. Z.Q. acknowledges the support from NSFC 22178389; S.M. acknowledges the support from NSFC 21975285; Z.Q. and S.M. acknowledge the support from PetroChina (PRIKY21084, KYWX-21-021).

6. Declaration of competing interest

The authors declare the compete interest for China Patent with application No. xxx.

7. Reference

[1] Bradley, S. A.; Broach, R. W.; Mezza, T. M.; Prabhakar, S.; Sinkler, W. Zeolite Characterization. In *Zeolites in Industrial Separation and Catalysis*. S. Kulprathipanja, Ed., 2010; pp 85-171.

[2] Liu, Z.; Zhou, J.; Tang, X.; Liu, F.; Yuan, J.; Li, G.; Huang, L.; Krishna, R.; Huang, K.; Zheng, A. Dependence of zeolite topology on alkane diffusion inside diverse channels. *AICHE J.* **2020**, *66*, e16269.

[3] Teketel, S.; Lundegaard, L. F.; Skistad, W.; Chavan, S. M.; Olsbye, U.; Lillerud, K. P.; Beato, P.; Svelle, S. Morphology-induced shape selectivity in zeolite catalysis. *J. Catal.* **2015**, *327*, 22-32.

[4] Hwang, Y. K.; Chang, J.-S.; Park, S.-E.; Kim, D. S.; Kwon, Y.-U.; Jhung, S. H.; Hwang, J.-S.; Park, M. S. Microwave fabrication of MFI zeolite crystals with a fibrous morphology and their applications. *Angew. Chem. Int. Ed.* **2005**, *44*, 556-560.

[5] Pagis, C.; Morgado Prates, A. R.; Farrusseng, D.; Bats, N.; Tuel, A. Hollow zeolite structures: An overview of synthesis methods. *Chem. Mater.* **2016**, *28*, 5205-5223.

[6] Opanasenko, M. V.; Roth, W. J.; Čejka, J. Two-dimensional zeolites in catalysis: current status and perspectives. *Catal. Sci. Technol.* **2016**, *6*, 2467-2484.

[7] Pérez-Ramírez, J.; Christensen, C. H.; Egeblad, K.; Christensen, C. H.; Groen, J. C. Hierarchical zeolites: enhanced utilisation of microporous crystals in catalysis by advances in materials design. *Chem. Soc. Rev.* **2008**, *37*, 2530-2542.

[8] Mintova, S.; Gilson, J.-P.; Valtchev, V. Advances in nanosized zeolites. *Nanoscale* **2013**, *5*, 6693-6703.

[9] Liu, X.; Shi, J.; Yang, G.; Zhou, J.; Wang, C.; Teng, J.; Wang, Y.; Xie, Z. A diffusion anisotropy descriptor links morphology effects of H-ZSM-5 zeolites to their catalytic cracking performance. *Commun. Chem.* **2021**, *4*, 107.

[10] Degnan, T. F.; Chitnis, G. K.; Schipper, P. H. History of ZSM-5 fluid catalytic cracking additive development at Mobil. *Microporous Mesoporous Mater.* **2000**, *35-36*, 245-252.

[11] Wise, J. J. Isomerization and disproportionation of alkyl aromatics. Patent US3377400A, 1968.

[12] Chen, N. Y. Personal perspective of the development of para selective ZSM-5 catalysts. *Ind. Eng. Chem. Res.* **2001**, *40*, 4157-4161.

[13] Hong, U.; Kärger, J.; Kramer, R.; Pfeifer, H.; Seiffert, G.; Müller, U.; Unger, K. K.; Lück, H. B.; Ito, T. PFG n.m.r. study of diffusion anisotropy in oriented ZSM-5 type zeolite crystallites. *Zeolites* **1991**, *11*, 816-821.

[14] Ji, Y.; Liu, Z.; Zhao, Z.; Gao, P.; Bao, X.; Chen, K.; Hou, G. Untangling framework confinements: A dynamical study on bulky aromatic molecules in mfi zeolites. *ACS Catal.* **2022**, 10.1021/acscatal.2c04646, 15288-15297.

[15] Choi, M.; Na, K.; Kim, J.; Sakamoto, Y.; Terasaki, O.; Ryoo, R. Stable single-unit-cell nanosheets of zeolite MFI as active and long-lived catalysts. *Nature* **2009**, *461*, 246-249.

[16] Jeon, M. Y.; Kim, D.; Kumar, P.; Lee, P. S.; Rangnekar, N.; Bai, P.; Shete, M.; Elyassi, B.; Lee, H. S.; Narasimharao, K.; Basahel, S. N.; Al-Thabaiti, S.; Xu, W.; Cho, H. J.; Fetisov, E. O.; Thyagarajan, R.; DeJaco, R. F.; Fan, W.; Mkhoyan, K. A.; Siepmann, J. I.; Tsapatsis, M. Ultra-selective high-flux membranes from directly synthesized zeolite nanosheets. *Nature* **2017**, *543*, 690-694.

[17] Guth, J. L.; Kessler, H.; Wey, R. New route to pentasil-type zeolites using a non alkaline medium in the presence of fluoride ions. *Stud. Surf. Sci. Catal.* **1986**, *28*, 121-128.

[18] Louis, B.; Kiwi-Minsker, L. Synthesis of ZSM-5 zeolite in fluoride media: an innovative approach to tailor both crystal size and acidity. *Microporous Mesoporous Mater.* **2004**, *74*, 171-178.

[19] Dai, W.; Kouvatas, C.; Tai, W.; Wu, G.; Guan, N.; Li, L.; Valtchev, V. Platelike MFI crystals with controlled crystal faces aspect ratio. *J. Am. Chem. Soc.* **2021**, *143*, 1993-2004.

[20] Zhang, J.; Ren, L.; Zhou, A.; Li, W.; Shang, S.; Liu, Y.; Jia, Z.; Liu, W.; Zhang, A.; Guo, X.; Song, C. Tailored synthesis of ZSM-5 nanosheets with controllable b-axis thickness and aspect ratio: Strategy and growth mechanism. *Chem. Mater.* **2022**, *34*, 3217-3226.

[21] Ban, T.; Mitaku, H.; Suzuki, C.; Matsuba, J.; Ohya, Y.; Takahashi, Y. Crystallization and crystal morphology of silicalite-1 prepared from silica gel using different amines as a base. *J. Cryst. Growth* **2005**, *274*, 594-602.

[22] Shi, J.; Zhao, G.; Teng, J.; Wang, Y.; Xie, Z. Morphology control of ZSM-5 zeolites and their application in Cracking reaction of C4 olefin. *Inorg. Chem. Front.* **2018**, *5*, 2734-2738.

[23] Liu, Y.; Qiang, W.; Ji, T.; Zhang, M.; Li, M.; Lu, J.; Liu, Y. Uniform hierarchical MFI nanosheets prepared via anisotropic etching for solution-based sub-100-nm-thick oriented MFI layer fabrication. *Sci. Adv.* **2020**, *6*, eaay5993.

[24] Ma, Q.; Fu, T.; Ren, K.; Li, H.; Jia, L.; Li, Z. Controllable orientation growth of ZSM-5 for methanol to hydrocarbon conversion: Cooperative effects of seed induction and medium pH control. *Inorg. Chem.* **2022**, *61*, 13802-13816.

[25] Liu, C.; Gu, W.; Kong, D.; Guo, H. The significant effects of the alkali-metal cations on ZSM-5 zeolite synthesis: From mechanism to morphology. *Microporous Mesoporous Mater.* **2014**, *183*, 30-36.
[26] Zhou, T.; Zhang, D.; Liu, Y.; Sun, Y.; Ji, T.; Huang, S.; Liu, Y. Construction of monodispersed single-crystalline hierarchical ZSM-5 nanosheets via anisotropic etching. *J. Energy Chem.* **2022**, *72*, 516-521.
[27] Huang, X.; Wang, C.; Zhu, Y.; Xu, W.; Sun, Q.; Xing, A.; Ma, L.; Li, J.; Han, Z.; Wang, Y. Facile synthesis of ZSM-5 nanosheet arrays by preferential growth over MFI zeolite [100] face for methanol conversion. *Microporous Mesoporous Mater.* **2019**, *288*, 109573.
[28] Qin, W.; Agarwal, A.; Choudhary, M. K.; Palmer, J. C.; Rimer, J. D. Molecular modifiers suppress nonclassical pathways of zeolite crystallization. *Chem. Mater.* **2019**, *31*, 3228-3238.
[29] Shang, Z.; Chen, Y.; Zhang, L.; Zhu, X.; Wang, X.; Shi, C. Plate-like MFI crystal growth achieved by guanidine compounds. *Inorg. Chem. Front.* **2022**, *9*, 2097-2103.
[30] Shan, Z.; Wang, H.; Meng, X.; Liu, S.; Wang, L.; Wang, C.; Li, F.; Lewis, J. P.; Xiao, F.-S. Designed synthesis of TS-1 crystals with controllable b-oriented length. *Chem. Commun.* **2011**, *47*, 1048-1050.
[31] Zhou, Z.; Jiang, R.; Chen, X.; Wang, X.; Hou, H. One-step synthesis of hierarchical lamellar H-ZSM-5 zeolite and catalytic performance of methanol to olefin. *J. Solid State Chem.* **2021**, *298*, 122132.
[32] Ali, B.; Lan, X.; Arslan, M. T.; Gilani, S. Z. A.; Wang, H.; Wang, T. Controlling the selectivity and deactivation of H-ZSM-5 by tuning b-axis channel length for glycerol dehydration to acrolein. *J. Ind. Eng. Chem.* **2020**, *88*, 127-136.
[33] Yang, J.; Gong, K.; Miao, D.; Jiao, F.; Pan, X.; Meng, X.; Xiao, F.; Bao, X. Enhanced aromatic selectivity by the sheet-like ZSM-5 in syngas conversion. *J. Energy Chem.* **2019**, *35*, 44-48.
[34] Qureshi, B. A.; Lan, X.; Arslan, M. T.; Wang, T. Highly active and selective nano H-ZSM-5 catalyst with short channels along b-axis for glycerol dehydration to acrolein. *Ind. Eng. Chem. Res.* **2019**, *58*, 12611-12622.
[35] Liu, Y.; Zhou, X.; Pang, X.; Jin, Y.; Meng, X.; Zheng, X.; Gao, X.; Xiao, F.-S. Improved para-Xylene Selectivity in meta-Xylene Isomerization Over ZSM-5 Crystals with Relatively Long b-Axis Length. *ChemCatChem* **2013**, *5*, 1517-1523.
[36] Shi, J.; Du, Y.; He, W.; Zhao, G.; Qin, Y.; Song, L.; Hu, J.; Guan, Y.; Zhu, J.; Wang, C.; Teng, J.; Xie, Z. Insights into the effect of the adsorption preference of additives on the anisotropic growth of ZSM-5 zeolite. *Chem. Eur. J.* **2022**, *28*, e202201781.
[37] Díaz, I.; Kokkoli, E.; Terasaki, O.; Tsapatsis, M. Surface structure of zeolite (MFI) crystals. *Chem. Mater.* **2004**, *16*, 5226-5232.
[38] Boxhoorn, G.; Sudmeijer, O.; van Kasteren, P. H. G. Identification of a double five-ring silicate, a possible precursor in the synthesis of ZSM-5. *J. Chem. Soc., Chem. Commun.* **1983**, 10.1039/C39830001416, 1416-1418.
[39] Hendricks, W. M.; Bell, A. T.; Radke, C. J. Effects of organic and alkali metal cations on the distribution of silicate anions in aqueous solutions. *J. Phys. Chem.* **1991**, *95*, 9513-9518.

[40] Camblor, M.; Mifsud, A.; Pérez-Pariente, J. Influence of the synthesis conditions on the crystallization of zeolite Beta. *Zeolites* **1991**, *11*, 792-797.
[41] Yue, Q.; Kutukova, K.; Li, A.; Čejka, J.; Zschech, E.; Opanasenko, M. Controllable zeolite AST crystallization: Between classical and reversed crystal growth. *Chem. Eur. J.* **2022**, *28*, e202200590.
[42] Khan, Z.; Rafiquee, M. Z. A.; Kabir-ud-din; Niaz, M. A.; Khan, A. A. Kinetics and mechanism of alkaline hydrolysis of urea and sodium cyanate. *Indian J. Chem., Sect. A: Inorg., Phys., Theor. Anal.* **1996**, *35*, 1116-1119.
[43] Price, G. D.; Pluth, J. J.; Smith, J. V.; Araki, T.; Bennett, J. M. Crystal structure of tetrapropylammonium fluoride-silicalite. *Nature* **1981**, *292*, 818-819.
[44] Grosskreuz, I.; Gies, H.; Marler, B. Alteration and curing of framework defects by heating different as-made silica zeolites of the MFI framework type. *Microporous Mesoporous Mater.* **2020**, *291*, 109683.
[45] Barlow, G. B.; Corish, P. J. Infrared absorption spectra of some urea complexes. *J. Chem. Soc.* **1959**, 10.1039/JR9590001706, 1706-1710.
[46] Piasek, Z.; Urbanski, T. The infra-red absorption spectrum and structure of urea. *Bull. Acad. Pol. Sci., Ser. sci. chim.* **1962**, *10*, 113-120.
[47] Tanaka, K.; White, J. M. Characterization of species adsorbed on oxidized and reduced anatase. *J. Phys. Chem.* **1982**, *86*, 4708-4714.
[48] Li, K.-M.; Jiang, J.-G.; Tian, S.-C.; Chen, X.-J.; Yan, F. Influence of silica types on synthesis and performance of amine–silica hybrid materials used for CO_2 capture. *J. Phys. Chem. C* **2014**, *118*, 2454-2462.
[49] Manivannan, M.; Rajendran, S. Investigation of inhibitive action of urea-Zn^{2+} system in the corrosion control of carbon steel in sea water. *Int. J. Eng. Sci. Technol.* **2011**, *3*, 8048-8060.
[50] Stewart, J. E. Infrared absorption spectra of urea, thiourea, and some thiourea‐alkali halide complexes. *J. Chem. Phys.* **1957**, *26*, 248-254.
[51] Cui, S.; Cheng, W.; Shen, X.; Fan, M.; Russell, A.; Wu, Z.; Yi, X. Mesoporous amine-modified SiO_2 aerogel: a potential CO_2 sorbent. *Energy Environ. Sci.* **2011**, *4*, 2070-2074.
[52] Patis, A.; Dracopoulos, V.; Nikolakis, V. Investigation of Silicalite-1 crystallization using attenuated total reflection/fourier transform infrared spectroscopy. *J. Phys. Chem. C* **2007**, *111*, 17478-17484.
[53] Al-Oweini, R.; El-Rassy, H. Synthesis and characterization by FTIR spectroscopy of silica aerogels prepared using several $Si(OR)_4$ and $R''Si(OR')_3$ precursors. *J. Mol. Struct.* **2009**, *919*, 140-145.
[54] Wang, Y.; Wang, R.; Xu, D.; Sun, C.; Ni, L.; Fu, W.; Zeng, S.; Jiang, S.; Zhang, Z.; Qiu, S. Synthesis and properties of MFI zeolites with microporous, mesoporous and macroporous hierarchical structures by a gel-casting technique. *New J. Chem.* **2016**, *40*, 4398-4405.
[55] Astorino, E.; Peri, J. B.; Willey, R. J.; Busca, G. Spectroscopic characterization of Silicalite-1 and titanium Silicalite-1. *J. Catal.* **1995**, *157*, 482-500.
[56] Iwasaki, A.; Sano, T.; Kiyozumi, Y. Effect of additives on the growth behavior of silicalite crystal. *Microporous Mesoporous Mater.* **1998**, *25*, 119-126.

Table of content